INTERNATIONAL JOURNAL OF AUTOMOTIVE AND MECHANICAL ENGINEERING
ISSN: 2229-8649 e-ISSN: 2180-1606
VOL. 20, ISSUE 3, 2023, 10684 – 10694
DOI: https://doi.org/10.15282/ijame.20.3.2023.11.0825

UNIVERSITI MALAYSIA PAHANG AL-SULTAN ABDULLAH

RESEARCH ARTICLE

Nonlinear Dynamics of a Multi-shaft Gear System in Parameter-state Space

Yan Yang[1,2,*]

[1]School of Mechatronic Engineering, Lanzhou Jiaotong University, 730070, Lanzhou, Gansu, China
[2]Key Laboratory of System Dynamics and Reliability of Rail Transport Equipment of Gansu Province, 730070, Lanzhou, Gansu, China

ABSTRACT - A nonlinear dynamic model of a 12-degree-of-freedom multi-shaft gear system is established, which includes nonlinear factors such as gear backlash, bearing clearance and time-varying mesh stiffness. The bifurcation diagrams and the maximum dynamic load coefficient diagrams that describe the dynamics of the gear transmission system are simulated by using the Runge-Kutta method, combined with three Poincaré mapping. The mutual transition of the adjacent period one motion through the grazing bifurcation and saddle-node bifurcation form a hysteresis zone where two types of impact motion coexist. The correlation between the dynamic response and the gear backlash under the parameter-state space is investigated, and it is verified that the extreme parameter conditions lead to abnormal vibration phenomena such as jumping, mesh-apart and chaotic motion. The results show that, near the critical value of ω = 0.7164 for grazing bifurcation, the meshing gear pair undergoes a jump in relative micro-displacement and dynamic load, increasing system impact vibration and a decrease in transmission efficiency, which is an undesirable parameter interval. In the initial stage of dynamic designing, the backlashes can be selected through the internal characteristics and transition mechanism of periodic motions.

ARTICLE HISTORY
Received : 12th May 2022
Revised : 06th July 2023
Accepted : 25th Aug 2023
Published : 09th Oct 2023

KEYWORDS
Nonlinear dynamics;
Meshing impact;
Bifurcation;
Hysteresis;
Dynamic load

1.0 INTRODUCTION

In mechanical equipment, the arrangement of multi-shaft transmission is generally adopted to achieve the functions of power and variable-speed transmission. A multi-stage transmission system contains multiple gears, whose nonlinear factors such as multi-clearances, time-varying mesh stiffness and comprehensive transmission error interact with one another; therefore, the system presents highly dimensional strong nonlinearity. In order to ensure a stable low noise stage condition when the multi-shaft transmission runs, it is necessary to study the connection between dynamics characteristics and design parameters in the system so that the optimization design scheme for global dynamic performance is obtained. Taking nonlinear factors such as external load excitation [1,2], relative damping ratio [3], and time-varying mesh stiffness [4,5] during gear meshing as objects, scholars have carried out a lot of research on the nonlinear dynamics of gear systems.

At present, the analytics method, the numerical simulation method and experimental verification are mainly used to solve the dynamics model of a gear transmission system. Kahraman [6] verified the applicability of the analytics method and the numerical simulation method in the nonlinear dynamics of gear rotor-bearing system based on comparing the agreement between theoretical data and experimental data. Sheng [7] used the Runge-kutta numerical integration method to solve the differential equation of planetary gear train motion, analyzed the influence of meshing frequency, meshing clearance, bearing clearance and other nonlinear parameters on the bifurcation and chaotic characteristics, and discussed the coupling effect of clearance on the nonlinear behavior of the system. Azimi [8] used the Poincare-Lindstedt method to study the dynamical parametric response of a one-stage spur gear pair with nonlinear suspension. It was found that pitchfork bifurcation and hopf bifurcation occurred around the primary and combination parametrically unstable tongues as the control parameters and meshing frequency varied and suggested that the selection of suitable suspension parameters could effectively prevent gear mesh-apart. Abruzzo [9] developed a gear lumped parameter model, numerically calculated the frequency response function of the tested gears, tested the transmission dynamic phenomena under different experimental conditions, and verified the correctness of the model and operations by comparing the numerical results with the measured values.

According to the method of tooth modification approach, Ullah [10] carried out the dynamic simulation of transmission error, safety factor and radial acceleration of the gearbox system and proposed the theoretical basis for the gear tooth micro-modification. Some research focuses on the dynamic load response of gear pairs under parametric excitation. Motahar [11], compares the effect of different optimized gear sets on the nonlinear dynamical behavior of gear systems, such as period-doubling bifurcation, by calculating the dynamic load coefficients of transmission gears. Xia [12] established a nonlinear dynamics model of a spur gear pair, used bifurcation diagrams, phase diagrams, and dynamic load calculations to obtain the motion state and dynamic response of the system, and analyzed the correlation between the dynamics parameters and the stability of the system under light and heavy load working conditions. Besides, the experimental method is also the key way to verify and correct the theoretical analysis of dynamic characteristics in the

*CORRESPONDING AUTHOR | Yan Yang | ✉ yany@mail.lzjtu.cn
© The Authors 2023. Published by Universiti Malaysia Pahang Publishing. This is an open access article under the CC BY-NC 4.0 license

gear system. Zhao, Rigaud, Martynenko and their co-workers [13-15] built vibration testing benches for different types of gear transmission systems and verified the accuracy and feasibility of system dynamics behavior by the diagrams of phase, bifurcation and time domain. With the development of nonlinear dynamics theories, Saghafi, Donmez, Arian, et al. [16-18] used the numerical simulation results of the gear system dynamic responses to study how to suppress or eliminate chaotic behavior.

The above nonlinear dynamics studies of gear systems are mainly based on the one-parameter bifurcation simulation analysis. However, carrying out multi-parameter and multi-performance co-simulation analysis can better reveal the non-smooth dynamic behavior formation mechanism of the gear transmission from the system level and guide the global dynamic performance matching design; some scholars have successively made exploratory studies on this. Farshidianfar [19] used nonlinear dynamic parameters such as backlash, load excitation, and time-varying stiffness as control parameters and explored the threshold surfaces for the bifurcation feature of the gear system in the control parameter space. Mason, and Gou [20,21] analyzed the global dynamic behavior of the gear single-stage model, constructed the collision mapping of gear meshing, and calculated the attraction basin, one-parameter and two-parameter bifurcation diagrams of the system.

The multi-parameter co-simulation of gear transmission is mostly carried out on single-stage gear, and the identification of meshing impact characteristics in the two-parameter plane is still unclear. Therefore, taking the gearbox of a type of locomotive, a dynamic model of a multi-shaft gear system is established based on the consideration of nonlinear factors such as radical clearance of rolling bearing, gear backlash, and time-varying mesh stiffness. Pattern types and transition mechanism of periodic impact motion groups in the system are resolved using the numerical integration method. The effects of jump behavior on the time-varying load of the meshing gear pair were investigated in this study. The periodic meshing impact of gear pair caused by the variations of backlash and diversity of the meshing state, including its evolution, are emphatically analyzed in parameter-state space.

2.0 METHODOLOGY

2.1 Model Description

The proposed dynamical model of the multi-shaft gear system shown in Figure 1 is derived from a specific locomotive gearbox. This model has the structure of a gear pairs transmission, consisting of an input gear 1, two output gears 2 and 3 and a fan transmission gear4, shafts and bearings. In the model, the friction during the meshing is not considered. The angular displacements of the input gear, the output gears and the fan transmission gear are respectively represented by θ_1, θ_2, θ_3 and θ_4. A rolling bearing that supports a gear is equivalent to a linear spring and linear damping, supporting stiffness coefficients in X and Y coordinates are represented by K_{ix}, K_{iy}, (i=1,2,3,4), supporting damping coefficients are represented by C_{ix}, C_{iy}, (i=1,2,3,4). Respectively, M_i, I_i, R_{bi}, (i=1,2,3,4) represent the mass, moment of inertia and base radius of each gear. The loads on the gear system in X and Y coordinates are represented by F_{ix}, F_{iy}, (i=1,2,3,4), respectively.

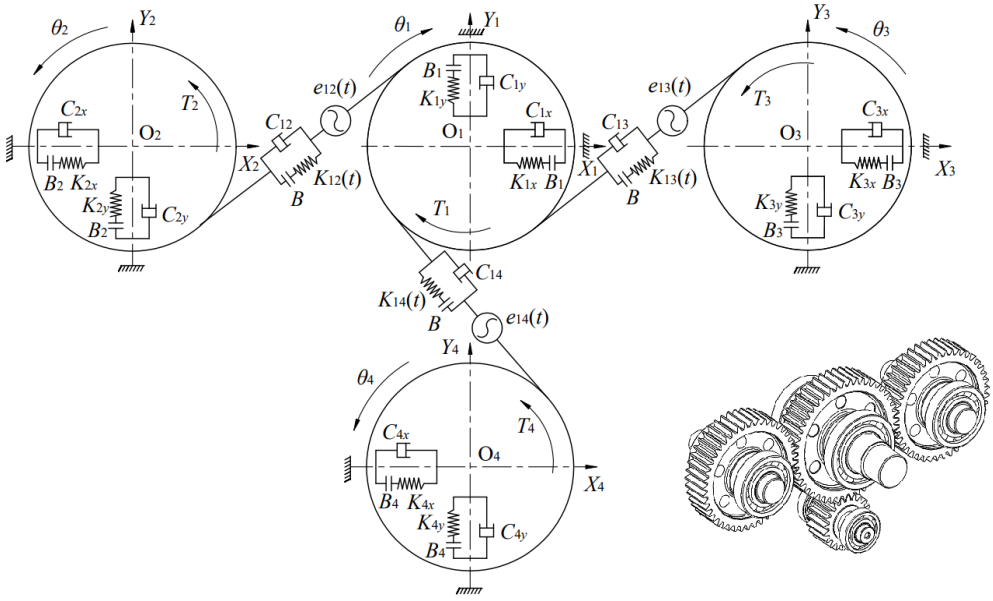

Figure 1. Dynamic model of the multi-shaft gear system

The multi-shaft gear system shown in Figure 1 under the input torque T_1, impedance torque T_2, T_3 and T_4, its bending-torsion coupling differential equations are represented as following Eq. (1):

$$\begin{cases} M_1\ddot{X}_1 + C_{1x}\dot{X}_1 + K_{1x}f_1(X_1, B_1) = -F_{2x} - F_{3x} - F_{4x} \\ M_1\ddot{Y}_1 + C_{1y}\dot{Y}_1 + K_{1y}f_1(Y_1, B_1) = -F_{2y} - F_{3y} - F_{4y} \\ I_1\ddot{\theta}_1 = T_1 - F_{2y}R_{b1} - F_{3y}R_{b1} - F_{4y}R_{b1} \\ M_2\ddot{X}_2 + C_{2x}\dot{X}_2 + K_{2x}f_2(X_2, B_2) = F_{2x} \\ M_2\ddot{Y}_2 + C_{2y}\dot{Y}_2 + K_{2y}f_2(Y_2, B_2) = F_{2y} \\ I_2\ddot{\theta}_2 = -T_2 + F_{2y}R_{b2} \\ M_3\ddot{X}_3 + C_{3x}\dot{X}_3 + K_{3x}f_3(X_3, B_3) = F_{3x} \\ M_3\ddot{Y}_3 + C_{3y}\dot{Y}_3 + K_{3y}f_3(Y_3, B_3) = F_{3y} \\ I_3\ddot{\theta}_3 = -T_3 + F_{3y}R_{b3} \\ M_4\ddot{X}_4 + C_{4x}\dot{X}_4 + K_{4x}f_4(X_4, B_4) = F_{4x} \\ M_4\ddot{Y}_4 + C_{4y}\dot{Y}_4 + K_{4y}f_4(Y_4, B_4) = F_{4y} \\ I_4\ddot{\theta}_4 = -T_4 + F_{4y}R_{b4} \end{cases} \quad (1)$$

The system has twelve degrees of freedom; the linear displacement degrees of freedom along the x and y coordinate axes are represented by X_i, Y_i (i=1,2,3,4), and rotational degrees of freedom are represented by θ_i (i=1,2,3,4). Their generalized coordinates can be expressed as$(X_1,Y_1,\theta_1,X_2,Y_2,\theta_2,X_3,Y_3,\theta_3,X_4,Y_4,\theta_4)^T$.

Radical clearance of the rolling bearing is decomposed in X and Y coordinate directions, which can be expressed by the nonlinear clearance function of Eq. (2):

$$f_i(X_i, B_i) = \begin{cases} X_i - B_i, (X_i > B_i) \\ 0, (-B_i \le X_i \le B_i) \\ X_i + B_i, (X_i < -B_i) \end{cases}, \quad f_i(Y_i, B_i) = \begin{cases} Y_i - B_i, (Y_i > B_i) \\ 0, (-B_i \le Y_i \le B_i), (i = 1,2,3,4) \\ Y_i + B_i, (Y_i < -B_i) \end{cases} \quad (2)$$

where, B_i represents half of the bearing radial clearance.

Relative micro-displacement of gear pairs 12, 13 and 14 at the meshing position along the meshing line direction due to the transmission errors and vibration are X_{12}, X_{13} and X_{14}, respectively, and their expressions are as follows.

$$X_{12} = -(X_1 - X_2)\sin\alpha_n + (Y_1 - Y_2)\cos\alpha_n + (\theta_1 R_{b1} - \theta_2 R_{b2})\cos\alpha_n - e_{12}(t) \quad (3)$$

$$X_{13} = (X_1 - X_3)\sin\alpha_n - (Y_1 - Y_3)\cos\alpha_n - (\theta_1 R_{b1} - \theta_3 R_{b3})\cos\alpha_n - e_{13}(t) \quad (4)$$

$$X_{14} = -(X_1 - X_4)\sin\alpha_n - (Y_1 - Y_4)\cos\alpha_n - (\theta_1 R_{b1} - \theta_4 R_{b4})\cos\alpha_n - e_{13}(t) \quad (5)$$

where, α_n is normal pressure angle. $e_{1j}(t)$ (j=2,3,4) is the comprehensive transfer error of gear pair, and can be expressed by the equation $e_{1j}(t)=E_{1j}\cos(\Omega t + \Psi_0)$. In the equation, E_{1j} represents the amplitude of transfer error, Ω represents the meshing angle frequency, $\Psi_0$represents the initial phase, and t represents the time. In Eq. (6), the time-varying meshing force on the gear teeth of gear 2, 3 and 4 is expressed as follows, along the X and Y coordinate directions.

$$\begin{cases} F_{2x} = -F_{12}(t)\sin\alpha_n \\ F_{2y} = F_{12}(t)\cos\alpha_n \end{cases}, \begin{cases} F_{3x} = F_{13}(t)\sin\alpha_n \\ F_{3y} = -F_{13}(t)\cos\alpha_n \end{cases}, \begin{cases} F_{4x} = F_{14}(t)\sin\alpha_n \\ F_{4y} = -F_{14}(t)\cos\alpha_n \end{cases} \quad (6)$$

where, $F_{12}(t)$, $F_{13}(t)$ and $F_{14}(t)$ are the time-varying dynamic loads during meshing, which can be expressed by the following Eq. (7):

$$F_{1j}(t) = K_{1j}(t)f(X_{1j}, B) + C_{1j}\ddot{X}_{1j}, (j=2,3,4) \quad (7)$$

In Eq. (7), the function of gear backlash is represented by $f(X_{1j},B)$ as the following equation:

$$f(X_{1j}, B) = \begin{cases} X_{1j} - B, (X_{1j} > B) \\ 0, (-B \le X_{1j} \le B) \\ X_{1j} + B, (X_{1j} < -B) \end{cases}, (j=2,3,4) \quad (8)$$

In Eq. (7), the time-varying meshing stiffness is represented by $K_{1j}(t)$, (j=2,3,4). It can be expressed as the equation $K_{1j}(t)=K_{mj} + K_a\cos(\Omega t + \Psi_0)$, where K_{mj} is the average meshing stiffness, and K_a is the amplitude of time-varying meshing stiffness. $C_{1j}(t)$, (j=2,3,4) represents the meshing damping and its expression is $C_{1j}=2C_{mj}\sqrt{K_{mj}M_{1j}}$, where C_{mj} is the relative damping ratio of meshing gear pair, and M_{1j} (j=2,3,4) is the equivalent mass of the gear pair, $M_{1j}=M_1M_j/(M_1+M_j) = I_1I_j/(I_1R_{bj}^2 + I_jR_{b1}^2)$.

Without loss of generality, the nominal dimension is defined as b_c, the inherent frequency as $\omega_n=\sqrt{K_m/M_{12}}$. Dimensionless parameters $x_i=X_i/b_c$, $y_i=Y_i/b_c$, $b_i=B_i/b_c$, $b=B/b_c$, $\tau=\omega_n t$, $\omega=\Omega/\omega_n$, $e_{12}(\tau)=e_{12}(t)/b_c$, $e_{13}(\tau)=e_{13}(t)/b_c$, $e_{14}(\tau)=e_{14}(t)/b_c$, $x_{12}=X_{12}/b_c$, $x_{13}=X_{13}/b_c$, $x_{14}=X_{14}/b_c$, (i=1,2,3,4) are introduced, where τ is the dimensionless time, and ω is the dimensionless meshing frequency.

The function of the dimensionless gear backlash is represented as the following equation:

$$f(x_{1j},b)=\begin{cases}x_{1j}-b,(x_{1j}>b)\\0,(-b\le x_{1j}\le b),\ (j=2,3,4)\\x_{1j}+b,(x<-b)\end{cases} \tag{9}$$

The function of the dimensionless radial clearance of the bearing is expressed as the following equation.

$$f_i(x_i,b_i)=\begin{cases}x_i-b_i,(x_i>b_i)\\0,(-b_i\le x_i\le b_i)\\x_i+b_i,(x_i<-b_i)\end{cases},\ f_i(y_i,B_i)=\begin{cases}y_i-b_i,(y_i>b_i)\\0,(-b_i\le y_i\le b_i)\\y_i+b_i,(y_i<-b_i)\end{cases},\ (i=1,2,3,4) \tag{10}$$

The above equations of dimensionless parameters are plugged into Eq. (1), and the following differential Eq. (11) of dimensionless motion of the system is obtained.

$$\begin{cases}\ddot{x}_1+2\xi_{1x}\dot{x}_1+k_{1x}f_1(x_1,b_1)-2a_1\xi_{21}\dot{x}_{12}-a_1k_{21}f(x_{12},b)+2a_1\xi_{31}\dot{x}_{13}+\\ \quad a_1k_{31}f(x_{13},b)+2a_1\xi_{41}\dot{x}_{14}+a_1k_{41}f(x_{14},b)=0\\ \ddot{y}_1+2\xi_{1y}\dot{y}_1+k_{1y}f_1(y_1,b_1)+2a_2\xi_{21}\dot{x}_{12}+a_2k_{21}f(x_{12},b)-2a_2\xi_{31}\dot{x}_{13}-\\ \quad a_2k_{31}f(x_{13},b)-2a_2\xi_{41}\dot{x}_{14}-a_2k_{41}f(x_{14},b)=0\\ \ddot{x}_2+2\xi_{2x}\dot{x}_2+k_{2x}f_2(x_2,b_2)+2a_1\xi_{12}\dot{x}_{12}+a_1k_{12}f(x_{12},b)=0\\ \ddot{y}_2+2\xi_{2y}y_2+k_{2y}f_2(y_2,b_2)-2a_2\xi_{12}\dot{x}_{12}-a_2k_{12}f(x_{12},b)=0\\ \ddot{x}_3+2\xi_{3x}\dot{x}_3+k_{3x}f_3(x_3,b_3)-2a_1\xi_{13}\dot{x}_{13}-a_1k_{13}f(x_{13},b)=0\\ \ddot{y}_3+2\xi_{3y}\dot{y}_3+k_{3y}f_3(y_3,b_3)+2a_2\xi_{13}\dot{x}_{13}+a_2k_{13}f(x_{13},b)=0\\ \ddot{x}_4+2\xi_{4x}\dot{x}_4+k_{4x}f_4(x_4,b_4)-2a_1\xi_{14}\dot{x}_{14}-a_1k_{14}f(x_{14},b)=0\\ \ddot{y}_4+2\xi_{4y}\dot{y}_4+k_{4y}f_4(y_4,b_4)+2a_2\xi_{14}\dot{x}_{14}+a_2k_{14}f(x_{14},b)=0\\ \ddot{x}_{12}+a_1(\ddot{x}_1-\ddot{x}_2)-a_2(\ddot{y}_1-\ddot{y}_2)+a_2^2k_{n2}f(x_{12},b)-2a_2^2\xi_{n2}\dot{x}_{12}-a_2^2k_{n3}f(x_{13},b)-\\ \quad 2a_2^2\xi_{n3}\dot{x}_{13}-a_2^2k_{n4}f(x_{14},b)-2a_2^2\xi_{n4}\dot{x}_{14}=a_2(f_{m1}+f_{m2})+\ddot{e}_{12}(\tau)\\ \ddot{x}_{13}-a_1(\ddot{x}_1-\ddot{x}_3)+a_2(\ddot{y}_1-\ddot{y}_3)-a_2^2k_{n2}f(x_{12},b)-2a_2^2\xi_{n2}\dot{x}_{12}+a_2^2k_{n3}f(x_{13},b)+\\ \quad 2a_2^2\xi_{n3}\dot{x}_{13}+a_2^2k_{n4}f(x_{14},b)+2a_2^2\xi_{n4}\dot{x}_{14}=-a_2(f_{m1}+f_{m3})+\ddot{e}_{13}(\tau)\\ \ddot{x}_{14}+a_2(\ddot{x}_1-\ddot{x}_4)+a_2(\ddot{y}_1-\ddot{y}_4)-a_2^2k_{n2}f(x_{12},b)-2a_2^2\xi_{n2}\dot{x}_{12}-a_2^2k_{n3}f(x_{13},b)-\\ \quad 2a_2^2\xi_{n3}\dot{x}_{13}+a_2^2k_{n4}f(x_{14},b)+2a_2^2\xi_{n4}\dot{x}_{14}=-a_2(f_{m1}+f_{m4})+\ddot{e}_{14}(\tau)\end{cases} \tag{11}$$

where, $\xi_{ix}=\frac{C_{ix}}{2M_i\omega_n}$, $\xi_{iy}=\frac{C_{iy}}{2M_i\omega_n}$, $k_{ix}=\frac{K_{ix}}{M_i\omega_n^2}$, $k_{iy}=\frac{K_{iy}}{M_i\omega_n^2}$, $\xi_{n2}=\frac{C_{12}}{2M_{12}\omega_n}$, $\xi_{n3}=\frac{C_{13}}{2M_{13}\omega_n}$, $\xi_{n4}=\frac{C_{14}}{2M_{14}\omega_n}$,$k_{n2}=\frac{K_{12}(\tau)}{M_{12}\omega_n^2}$, $k_{n3}=\frac{K_{13}(\tau)}{M_{13}\omega_n^2}$, $k_{n4}=\frac{K_{14}(\tau)}{M_{14}\omega_n^2}$, $\xi_{12}=\frac{\xi_{n2}M_{12}}{M_2}$, $\xi_{13}=\frac{\xi_{n3}M_{13}}{M_3}$, $\xi_{14}=\frac{\xi_{n4}M_{14}}{M_4}$, $\xi_{21}=\frac{\xi_{n2}M_{12}}{M_1}$, $\xi_{31}=\frac{\xi_{n3}M_{13}}{M_1}$, $\xi_{41}=\frac{\xi_{n4}M_{14}}{M_1}$, $k_{12}=\frac{k_{n2}M_{12}}{M_2}$, $k_{13}=\frac{k_{n3}M_{13}}{M_3}$, $k_{14}=\frac{k_{n4}M_{14}}{M_4}$, $k_{21}=\frac{k_{n2}M_{12}}{M_1}$, $k_{31}=\frac{k_{n3}M_{13}}{M_1}$, $k_{41}=\frac{k_{n4}M_{14}}{M_1}$, $f_{m1}=\frac{T_1}{M_1\omega_n^2b_cR_{b1}}$, $f_{m2}=\frac{T_2}{M_2\omega_n^2b_cR_{b2}}$, $f_{m3}=\frac{T_3}{M_3\omega_n^2b_cR_{b3}}$, $f_{m4}=\frac{T_4}{M_4\omega_n^2b_cR_{b4}}$, $\ddot{e}_{12}(\tau)=-e_{m2}\omega^2\cos(\omega\tau+\psi_0)$, $\ddot{e}_{13}(\tau)=-e_{m3}\omega^2\cos(\omega\tau+\psi_0)$, $\ddot{e}_{14}(\tau)=-e_{m4}\omega^2\cos(\omega\tau+\psi_0)$, $a_1=\sin\alpha_n$, $a_2=\cos\alpha_n$, (i=1,2,3,4).

2.2 Poincaré Sections and Simulation Data

The main standard designing parameters for the multi-shaft gear system with multi-clearances are; the modulus m=7 mm, the gear teeth number of input gear z_1=49, the gear teeth number of output gear z_2=z_3=44, the gear teeth number of fan transmission gear z_4=21, and the normal pressure angle α_n=20°. The standard dynamic parameters are selected in Table 1.

Table 1. Dynamics parameters of the system

Dynamic parameter	Symbol	Value	Remark
Displacement nominal dimension/m	b_c	50×10^{-6}	
Gear backlash/m	$2B$	100×10^{-6}	
Bearing radial clearance/m	$2B_i$	100×10^{-6}	(i=1,2,3,4)
Input torque /N·m	T_1	800	
Comprehensive transmission error /m	E_{mj}	25×10^{-6}	(j=2,3,4)
Support stiffness in X,Y coordinate direction / N·m^{-1}	K_{ix},K_{iy}	2.0×10^{7}	(i=1,2,3,4)
Average meshing stiffness /N·m^{-1}	K_{mj}	2.6×10^{8}	(j=2,3,4)
Time-varying meshing stiffness amplitude	K_a	0.2	
Support damping ratio	ζ_{ix},ζ_{iy}	0.1	(i=1,2,3,4)
Meshing damping ratio	C_{mj}	0.1	(j=2,3,4)

Three Poincaré sections are defined to describe the impact characteristics of the gear system:

i. Meshing periodic mapping section: $\sigma_n=\{(\tau,x,\dot{x})\in R^2\times T|\tau=\mathrm{mod}(2\pi/\omega)\}$
ii. Tooth surface impact mapping section: $\sigma_p=\{(\tau,x,\dot{x})\in R^2\times T|x=b\}$
iii. Tooth back impact mapping section: $\sigma_q=\{(\tau,x,\dot{x})\in R^2\times T|x=-b\}$

By the periodic mapping σ_n, the motion period number n of the excitation force contained in a meshing period T=$2n\pi/\omega$ can be determined. Through the tooth surface impact mapping σ_p and tooth back impact mapping σ_q, the numbers of tooth

surface impact and back impact, namely p and q are respectively determined. Combined with three types of Poincare mapping, the periodic motion pattern of the gear pair is obtained. The dimensionless differential equation in Eq. (11) is solved using the fourth-order Runge-Kutta numerical integration with variable step size, and the global bifurcation diagram, phase diagram, Poincaré projection mapping and the maximum dynamic load coefficient are obtained under standard parameters. Accordingly, nonlinear dynamic characteristics of the gear system are analyzed.

3.0 RESULTS AND DISCUSSION

3.1 Nonlinear Dynamics under Standard Parameters

During the meshing process, there are generally three impact states on the meshing gear teeth [22], which are expressed by the symbol I. I=0 means the non-impact state, also called complete meshing condition, that the driving tooth and driven tooth of the gear pair are always in contact without separation. In this state, the system runs linearly. I=1 means the unilateral impact state that the impact occurs on the forward surface of the driving tooth or the backward surface of the driven tooth, the driving tooth and driven tooth of the gear pair separated. I=2 means the bilateral impact state that the impacts simultaneously occur on the forward and backward surface of the tooth in one meshing period or alternately occur in several meshing periods.

Additional dynamic loads or impacts are generated during meshing because of the manufacture and assemble errors, elastic deformation of gear teeth, and time-varying characteristics of meshing stiffness accompanied by the alternate occurrence of single and double tooth mesh of gear pairs [23,24]. Dynamic load coefficient K_v is usually used to evaluate the deviation of the actual dynamic load from the theoretical load in the gear dynamics studies. The dynamic load during the meshing is variable by time, so the dynamic load coefficients in each meshing period (T=2$n\pi/\omega$) were continuously sampled. The maximum in the date set obtained is exactly the maximum dynamic load coefficient $K_{v\max}$ at the motion state. The larger the value of $K_{v\max}$ is, the greater the alternating impact stress and the more serious the impact noise is.

Under standard parameters, the dimensionless meshing frequency ω is set as the control parameter, and the global bifurcation diagrams of gear pair 12, 13 and 14 are shown in Figures 2(a), 2(b) and 2(c), respectively. In the figures, the state of I=0 non-impact is shown in red, I=1 unilateral impact in black, and I=2 bilateral impact in blue. It can be observed that with the variations of controlling parameters ω, the periodic motion pattern and the bifurcation law is consistent, except for the amplitudes of relative micro-displacement at the meshing position. Therefore, in this study, gear pair 12 is focused on typically describing the dynamic characteristics of a multi-shaft gear system. As shown in Figure 2(d), the maximum dynamic load coefficient $K_{v\max}$ during the meshing gear pairs varies with the controlling parameters ω.

Taking $\omega\in$[0.712, 0.72] as the simulation interval, Figure 3 describes the mutual transition between the adjacent 1-0-0 and 1-1-0 impact motion of gear pair 12. The irreversibility of the adjacent impact motions mutual transition and the formation process of the hysteresis zone are discussed based on this. The superscript "$\leftrightarrow$" of the control parameter ω in Figure 3 indicates the superposition of increasing and decreasing directions of ω during the numerical calculation. With the meshing frequency ω increases, the period 1 non-impact motion 1-0-0 transfers into the period 1 one-sided tooth surface impact motion 1-1-0 through the grazing bifurcation point $G_{1\text{-}0\text{-}0}$ (ω=0.7164). The relative micro-displacement x_{12} jumps after the bifurcation point $G_{1\text{-}0\text{-}0}$. On the contrary, with the meshing frequency ω decreases, the 1-1-0 one-sided impact motion passes through the saddle-node bifurcation point $SN_{1\text{-}1\text{-}1}$ (ω=0.8448) into 1-0-0 non-impact motion. A narrow hysteresis zone $L_{1\text{-}0\text{-}0}\cap L_{1\text{-}1\text{-}0}$ is formed between the bifurcation points $G_{1\text{-}0\text{-}0}$ and $SN_{1\text{-}1\text{-}1}$; within this hysteresis zone, adjacent 1-0-0 and 1-1-0 period 1 motions coexist simultaneously and stably. The control parameter ω passes through the hysteresis zone from the bifurcation point $G_{1\text{-}0\text{-}0}$, and the meshing gear tooth surface impact number p increases by 1. Conversely, ω leaves the hysteresis zone through the bifurcation point $SN_{1\text{-}1\text{-}1}$, the impact number p is reduced by 1, and the excitation force period number n=1 in a meshing period remains unchanged.

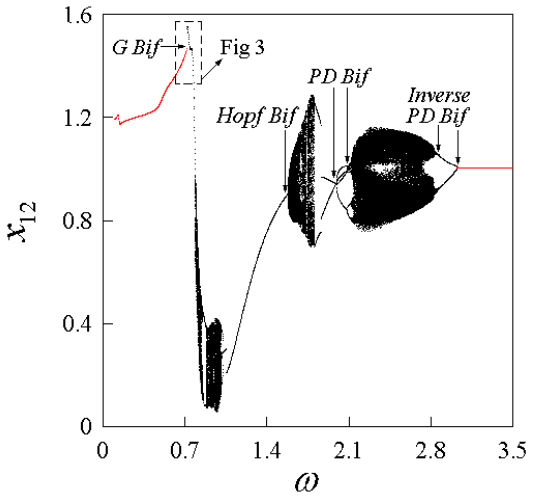

(a) bifurcation diagram of gear pair 12

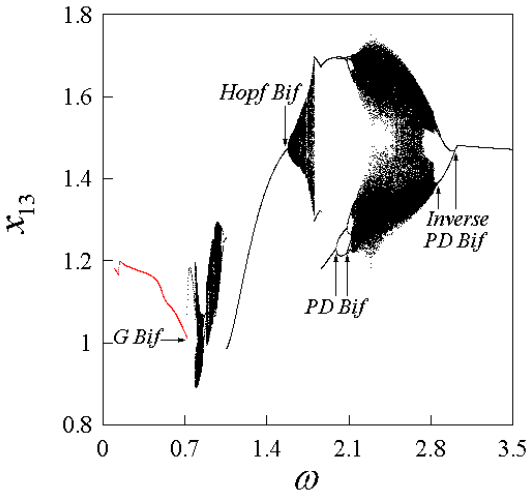

(b) bifurcation diagram of gear pair 13

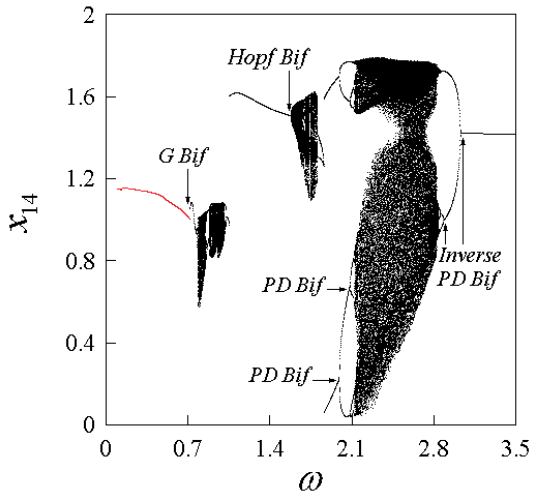

(c) bifurcation diagram of gear pair 14

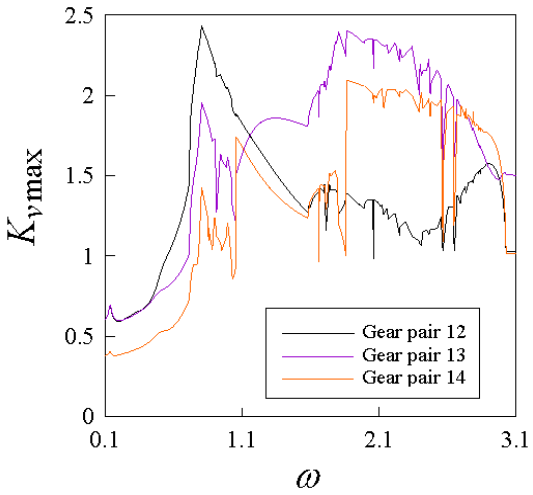

(d) maximum dynamic load coefficient $K_{v\max}$ of gear pairs 12,13 and 14

Figure 2. Global bifurcation and the maximum dynamic load coefficient diagrams of the gear pairs

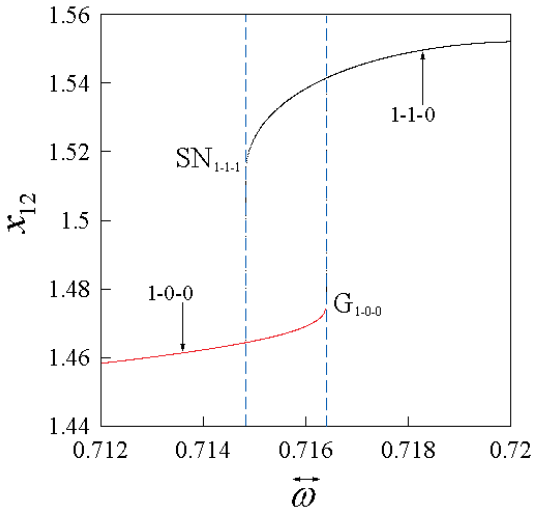

Figure 3. Transitions between 1-0-0 motion and 1-1-0 motion

From Figure 2, the gear pair 12, 13 and 14 both exhibit a state of full meshing in period 1 of 1-0-0 stage when ω is in the low-frequency domain. From Figure 4(a), the phase diagram of gear 12 is a closed curve, and the Poincaré mapping of phase trajectory over periodic σ_n is a point in red, along with the stable run and lower vibration noise of gear transmission. With an increase in meshing frequency ω, the relative micro-displacement x_{12} increases. When ω exceeds 0.7164, for gear pair 12, the state changes from non-impact complete meshing motion in the 1-0-0 stage to unilateral tooth surface impact motion in the 1-1-0 stage, grazing bifurcation (which are marked as "G Bif" in Figure 2) occurring, with the number of the period is the constant 1, which is shown in Figure 4(b). Grazing causes the system to jump around the bifurcation critical value of the control parameter ω in Figure 4(c). The 1-1-0 motion pattern does not change with the jump; however, as a reference in Figure 2(d), the maximum dynamic load coefficient increases abruptly due to the suffering of instantaneous impact at the meshing position, causing harm to meshing teeth, in serious cases, even damage to teeth or transmission failure. With the meshing frequency ω increases into the intermediate frequency domain, the 1-1-0 unilateral tooth surface impact motion firstly enters quasi-periodic impact motion through Hopf bifurcation (Hopf Bif), then the quasi-periodic motion transits to long-period multi-impact motion and chaotic motion via phase locking.

As shown in Figure 4(d), the phase diagram of chaotic motion presents multiple intersecting curve trajectories, and there are many scattered points in the mapping section σ_n. Due to the inherent sensitivity and randomness of the initial value, chaotic motion makes the gear system seriously unstable, the impact number on the tooth surface increases sharply, and the impact noise intensifies. Therefore, in the early stage of gear design, it is necessary to avoid the system working in the corresponding chaos frequency range to ensure the stable operation of the gear system. With a further increase in ω, the system degenerates from chaos into 2-1-0, 2-2-0 motion; when ω=1.89, the jump phenomenon occurs again near the grazing bifurcation point $G_{2\text{-}1\text{-}0}$ between the above two motions. The phase path of 2-2-0 motion crosses σ_n twice to form two stable projection points in Figure 4(e). 4-4-0 motion is generated by period-doubling bifurcation (PD Bif) with

an increase in ω. When ω crosses 2.05, the gear pair 12 passes through the saddle-node bifurcation point $SN_{4\text{-}4\text{-}0}$. At this time, the phase trajectory grazes at backlash b=1 shown in Figure 4(f), and the number of tooth surface impacts is reduced by 1, which produces the 4-3-0 impact motion. After a long window of chaotic motion as in Figure 4(g), gear pair 12 gradually degenerates into 8-4-0, 4-2-0, 2-1-0 motion through a series of inverse period-doubling bifurcations (Inverse PD Bif) with increasing ω, see Figure 4(h). The phase diagram shows continuous inverse doubling of the period number n, and the number of projection points is respectively 8, 4 and 2. Eventually, the meshing impact motion changes to a stable 1-1-0 state, see Figure 4(i). In this process, the relative micro-displacement x_{12} decreases continuously; the maximum dynamic load coefficient decreases continuously, the impact number and noise decrease, and the stability gradually improves.

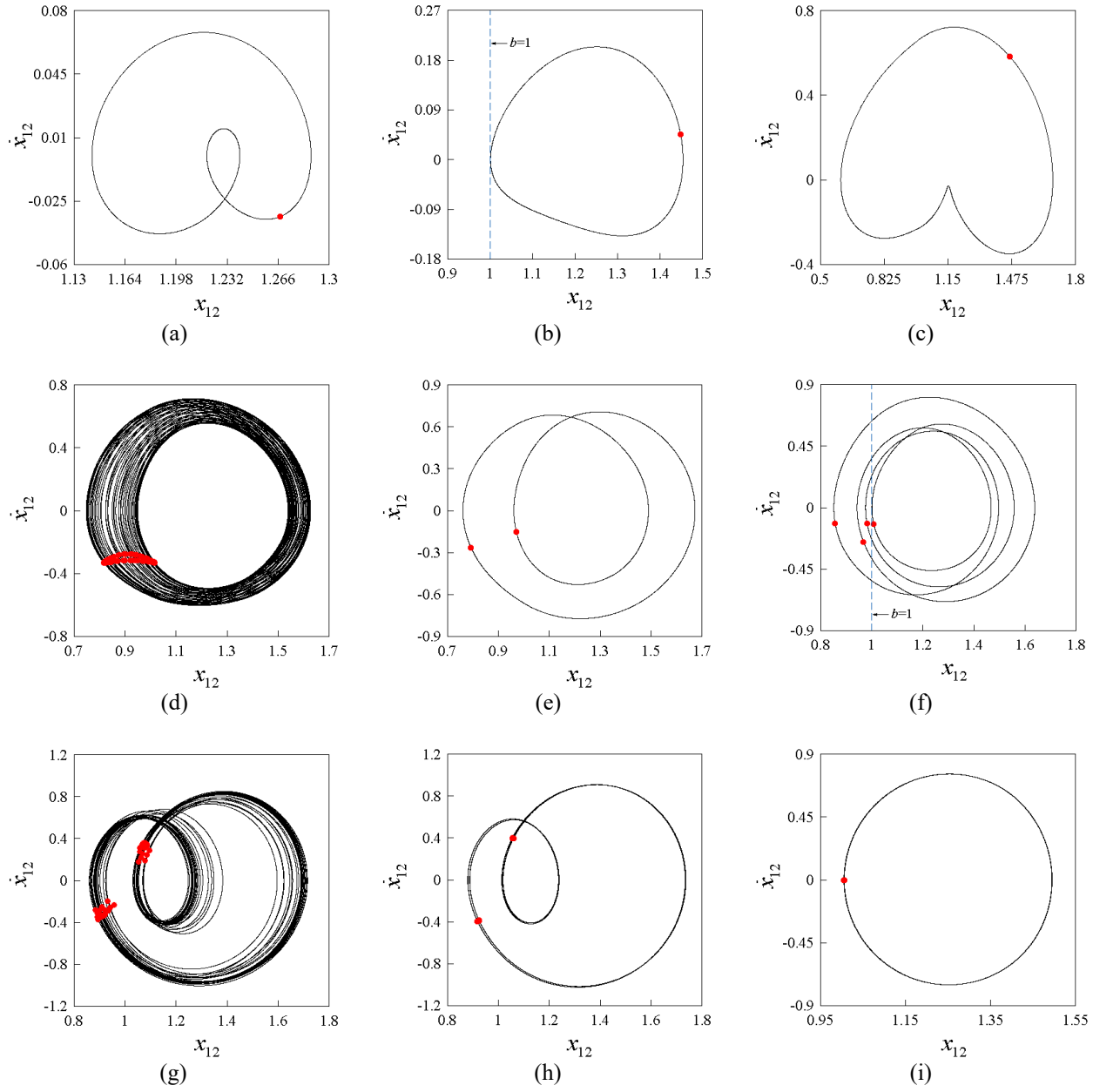

Figure 4. Superpositions of phase diagram and Poincaré mapping of the gear pair12: (a) ω=0.5, 1-0-0 motion; (b) ω=0.7164, 1-0-0 grazing bifurcation; (c) ω=0.75, 1-1-0 motion; (d) ω=1.6, chaotic motion; (e) ω=1.89, 2-2-0 motion; (f) ω=2.05,4-4-0 Saddle-node bifurcation; (g) ω=2.8, chaotic motion; (h) ω=2.856, 16-12-0 motion; (i) ω=3.1, 1-1-0 motion

3.2 Effects of Backlash on Gear System Dynamics

Through synergistic simulation based on multi-parameter and multi-performance, the dynamic response and dynamic parameters matching rules of gear system can be studied from the system level, which provides a theoretical basis for system dynamic design. This study focuses on the meshing impact characteristics of gear system under the superposition of multiple stages backlashes. In this section, we study the dynamic characteristics of the gear system by taking the meshing frequency ω and the gear backlash b as control parameters with a region of $b\in[0, 1]$, $\omega\in[0.1, 3.1]$ and keeping other standard parameters constant. In Figure 5(b) to 5(d), the parameter domain and distribution law of the periodic

meshing motion in the (ω,b) parameter-state space are obtained through numerical simulation and represented by different colors and symbol nT-I (the meshing period nT,$n \geq 1$; the impact state I=0,1,2). The gray and not marked areas are irregular motion, long-periodic multi-impact motion or chaotic motion in the figures. The three-dimensional diagrams shown in Figure 5(a) contain 30 single-parameter bifurcation diagrams with relative micro-displacement x_{12}; each bifurcation diagram corresponds to a certain backlash parameter b, which reflects the relationship between the relative micro-displacement x_{12} and the dynamic parameters (ω,b).

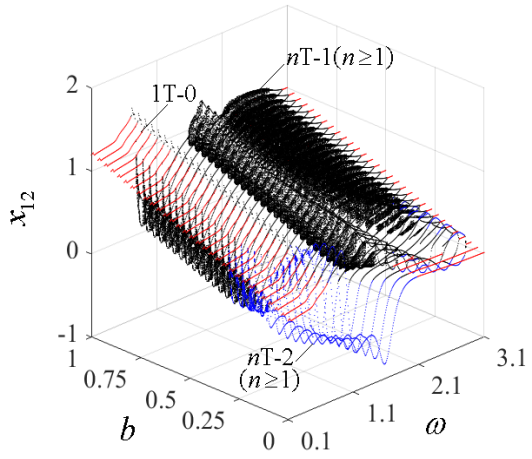

(a) bifurcation diagram of relative micro-displacement x_{12}

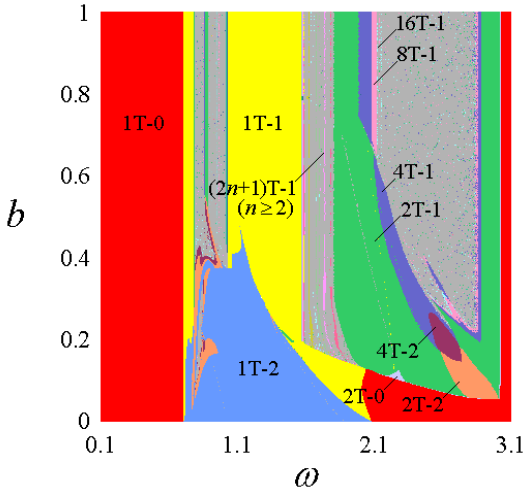

(b) distribution domains of impact motions for gear pair 12

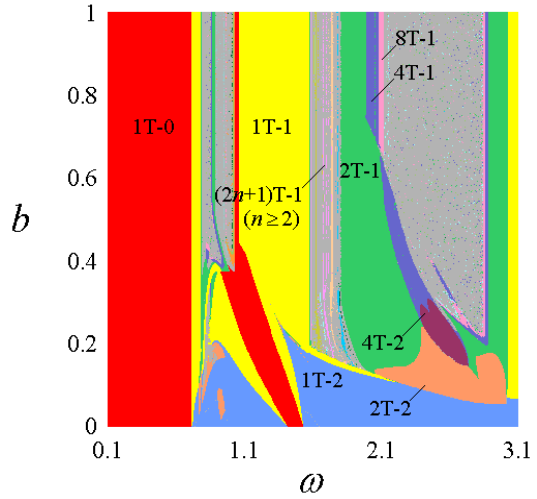

(c) distribution domains of impact motions for gear pair 13

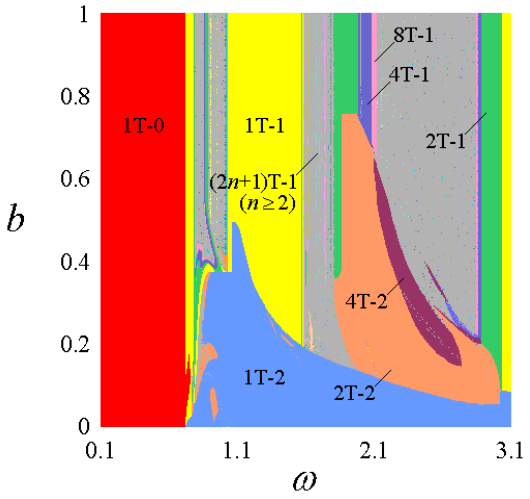

(d) distribution domains of impact motions for gear pair 14

Figure 5. (ω,b) parameter-state diagrams showing the distributions and transition law of periodic motions for the gear pairs

It can be seen from Figure 5(b) to 5(d) that in the (ω,b) parameter-state space, the three gear pairs mainly present three meshing motions: 1T-0 non-impact, nT-1 unilateral tooth surface impact, and nT-2 bilateral impact. In the low-frequency domain, the relative micro-displacement exhibits a linear jump behavior at the meshing position, and the jump bifurcation value is independent of gear backlash b. As shown in Figure 5(b), in the small gear backlash domain, gear pair 12 enters bilateral impact motion from the narrow period 1 non-impact motion, which seriously affects the critical speed of the "meshing-impact" jump. In the low-frequency and large backlash region, the meshing gear pair 12 presents 1T-0 motion with complete meshing and no impact, and the meshing relative micro-displacement x_{12} is always greater than the backlash. The two meshing tooth surfaces are always in contact with each other and not be separated. With an increase in ω, 1T-0 non-impact motion undergoes grazing bifurcation and transits to 1T-1 unilateral impact motion parameter domain without changes in the motion period n. It can be seen a grazing bifurcation line between the red (1T-0) and the black (nT-1) area in Figure 5(a), which corresponds to the boundary between 1T-0 motion and 1T-1 motion parameter domains in Figure 5(b). Grazing bifurcation of 1T-0 motion corresponds to stability boundary $G_{1T\text{-}0}$, and 1T-1 motion stabilizes after a jump transition. On the jump boundary $J_{1T\text{-}0/1T\text{-}0}$ between adjacent impact state parameter domains, the meshing displacement of the gear pair increases suddenly, which has a great influence on the dynamic load. Gear pair 12 exhibits

1T-2 bilateral swing impact characteristics in the small backlash region, which leads to the operation stability of the gear system being reduced, the driving ability weaker, and the impact noise higher. With increasing the meshing frequency ω, a parameter island consisting of 2T-2, 4T-2 double-sided impact motions appear and gradually decreases with increasing b. In the upper right region of the (ω,b) parameter-state space, a series of period-doubling bifurcations occur with increasing the meshing frequency ω, and induce a group of 2T-1、4T-1、8T-1 unilateral impact motions. After ω>2.835, the transition process of the meshing impact motion for gear pair 12 is: nT-1→16T-1→8T-1→4T-1→2T-1→1T-0, in this meshing frequency range, the type of meshing period motion does not change with increasing in backlash b, only the meshing relative micro-displacement increases linearly. In conclusion, it can be seen that the backlash b is mainly reflected in the small value range as a strong nonlinear factor of the gear system, which will result in bilateral impact motion.

Because of the coupling effect between the gear pairs, the pattern type of meshing impact motion and bifurcation characteristics of gear pairs 13 and 14 shown in Figures 5(c)-(d) are similar to the gear pair 12. The difference is: a) The gear pairs 13 and 14 do not transit into 1T-0 non-impact motion in the high-frequency domain but maintain the 1T-1 unilateral tooth surface impact motion state. 1T-2 bilateral impact motion parameter domain moves in the direction of increasing meshing frequency; b). 1T-2 parameter domain of the gear pair 13 in the small clearance range is divided into two parts by 1T-0 and 1T-1 motions, and the peak value of 1T-2 motion parameter domain corresponding to the backlash b is significantly reduced; c). 4T-1, 2T-1 motion parameter domain of gear pair 14 is extended to the large backlash range, the window of I=2 bilateral impact motion parameter domain in the (ω,b) parameter-state space increases, and the undesirable parameter range for severe meshing impact increases.

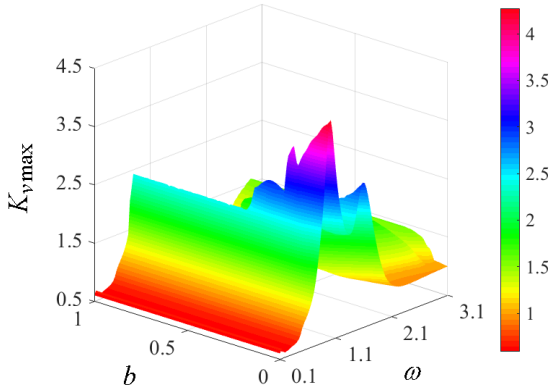

Figure 6. Parameter-state diagrams showing the maximum dynamic load coefficient K_{vmax} of the gear pair 12 in the (ω,b) parameter-state space

According to the definition of the maximum dynamic load coefficient K_{vmax}, the 3D surface diagram of K_{vmax} for gear pair 12 in the (ω,b) parameter-state space is obtained in Figure 6, which intuitively reflects the distribution of the maximum dynamic load coefficient in the two-parameter control domain. In the 1T-0 non-impact complete meshing domain, the maximum dynamic load coefficient K_{vmax} of the gear pair 12 is less than 0.75. With the increase of meshing frequency ω, K_{vmax} fluctuates with the dynamic behaviors such as jump, grazing bifurcation or period-doubling bifurcation. Corresponding I=1 unilateral tooth surface impact motion parameter domain in Figure 5(b), K_{vmax} mainly presents a distribution state parallel to the coordinate axis of backlash b, the dynamic performance of the gear system is approximately linear, and the impact state does not change with b. On the jump boundary, $J_{1T\text{-}0/1T\text{-}0}$, the maximum dynamic load coefficient K_{vmax} of the gear pair 12 increases sharply at ω=0.7164. In the chaotic motion and the small backlash domain with I=2 bilateral impact parameter domain, the meshing motion exhibits strong nonlinear characteristics, the dynamic load fluctuates with the change of backlash, and K_{vmax} continues to increase to a peak value of K_{vmax}>4. It shows that the alternating stress of the meshing gear teeth is larger in this interval, and the tooth surface impact is stronger.

During a horizontal scan of changing meshing frequency ω through different pattern types of impact motion regions, the diversity and evolution of the meshing characteristics can be observed by the single-parameter bifurcation diagrams. Figure 7 shows the relative micro-displacement x_{12} bifurcation diagram of the meshing gear pair 12 under different values of the dimensionless backlash b. By analyzing the stability and bifurcation of periodic motion, its parameter domain distribution and boundary line in the two-dimensional parameter plane can be described in detail. It can be seen from Figure 7(a) to 7(c) that when the value of dimensionless gear backlash b is different, complex nonlinear impact characteristics emerge in the gear system, and the system is sensitive to the parameter of gear backlash. Comparing with the calculation results under standard parameters in Figure 2(a), as shown in Figure 7(a), in the limit state where the dimensionless gear backlash b is 0.2, the meshing gear pair 12 has two windows of bilateral impact motions respectively, showing 1T-2 motion in $\omega \in$ [0.739, 1.459] and 4T-2 motion in $\omega \in$ [2.539, 2.692]. From Figure 7(b), when the dimensionless gear backlash b increases to 0.35, the bilateral impact window of the system becomes narrower to the interval of $\omega \in$ [0.79, 1.207], and the impact motion mode in the high-frequency domain mainly exhibits as I =1 unilateral impact motion state. The bilateral impact behavior leads to an increase in the relative displacement of meshing gear teeth

on the tooth back, and reduces the fatigue life of the gear. As shown in Figure 7(c), when b equals to 0.75, the bilateral impact state of the meshing gear pair disappears. In the middle and high-frequency domain, the chaotic motion window moves to the region where the frequency increases.

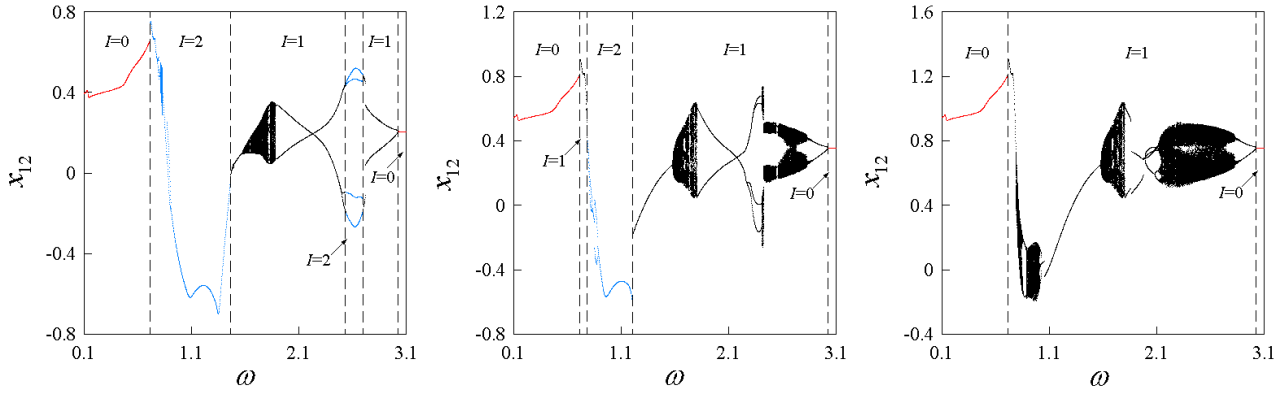

(a) b=0.2 (b) b=0.35 (c) b=0.75

Figure 7. Bifurcation diagrams of relative micro-displacement x_{12} under different dimensionless backlash b

The following analyses are associated with the selected parameters: gear backlash b=0.35 and meshing frequency ω=1.05. In Figure 8(a), the meshing trajectory of gear pair 12 goes through the σ_n mapping once, forming and 1 fix points on the meshing periodic Poincaré section. The tooth surface impact occurs once under b equaling 0.35, and the tooth back impact occurs once under b equaling -0.35. As shown in the responding diagram of the time domain to relative micro-displacement x_{12} (Figure 8(b)), both tooth surface impact and tooth back impact occur simultaneously under this condition. As shown in Figure 8(c), the responding curve of the time domain to dynamic load coefficient K_v is irregular, showing positive, zero and negative values. When the dynamic load coefficient K_v equals 0, the meshing gear teeth bear alternating dynamic loads. If the system runs in this parameter range for a long time, it is easy to produce tooth root fatigue fracture or tooth surface damage. It can be seen that the gear backlash is an important factor affecting the meshing impact characteristics and mesh-apart. What needs to be paid attention to is that in a meshing period, the more times of impact on the tooth surface and tooth back, the more obvious the adverse effects of vibration and noise caused by impact.

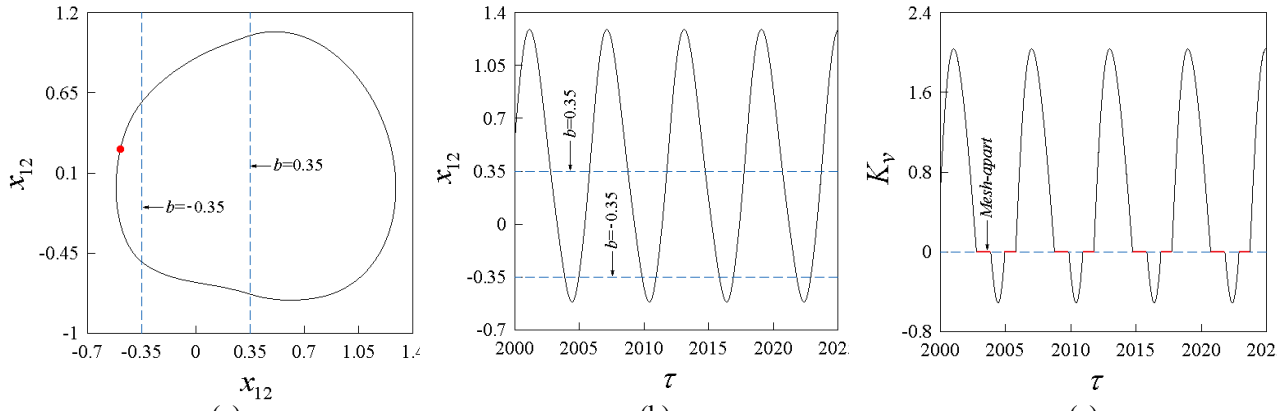

(a) (b) (c)

Figure 8. 1-1-1 double-sided impact motion, when b=0.35, ω=1.05: (a) phase diagram; (b) time response of relative micro-displacement x_{12} and (c) time response of dynamic load coefficient K_v

From the above analysis, it can be seen that the meshing frequency ω=0.7164 is the critical value for the jumping behavior of the meshing gear pair. When the gear backlash b is large, ω is in the region of [0.79,1.0], [1.58,1.8], and [2.125,2.85], the gear system is in the state of chaotic motion and long-period impactic motion, and the input speed can be adjusted to prevent the gear system from continuously operating in this state domain.

4.0 CONCLUSIONS

Based on the consideration of the nonlinear factors, including bearing radical clearances, gear backlashes, and time-varying meshing stiffness, a nonlinear time-varying model of the multi-shaft gear system is established. The pattern types and bifurcation characteristics of meshing impact motion under external load excitation are studied. The main conclusions are drawn as follows.

i. The multi-shaft gear system is a strong nonlinear dynamic system with multiple degrees of freedom, and the system mainly presents non-impact motion in the low-frequency domain.

ii. Grazing bifurcation of the meshing gear pair occurs with increasing frequency, and the complex dynamic characteristics of the local area near the grazing bifurcation point are analyzed to reveal the irreversibility of mutual transitions between adjacent fundamental periodic motions. The two types of adjacent impact motions in the hysteresis domain coexist stably.

iii. Near the grazing bifurcation boundary ω=0.7164, there is a jump in the relative micro-displacement of the gear pair and a sudden increase in dynamic load, which causes a hard impact on the tooth surface, so this parameter condition is not an optional sensitive area.

Extreme parameter conditions lead to abnormal vibration phenomena such as jumps, double-sided impact, dynamic mesh-apart and chaotic motion. A reasonable combination of design parameters can avoid the abnormal vibration state domain of the gear system and effectively reduce the dynamic instability of the gear pair caused by excessive meshing impacts.

5.0 ACKNOWLEDGEMENT

The authors gratefully acknowledge the support of the National Natural Science Foundation of China (12162019) and Gansu Science and Technology Planning Project (21JR7RA307, 21YF5WA060).

6.0 REFERENCES

[1] A. Mélot, Y. Benacha, E. Rigaud, J. Perret-Liaudet, and F. Thouverez, "Effect of gear topology discontinuities on the nonlinear dynamic response of a multi-degree-of-freedom gear train," *Journal of Sound and Vibration*, vol. 516, pp. 116495, 2022.

[2] L. Ryali, and D. Talbot, "Dynamic load distribution of planetary gear sets subject to both internal and external excitations," *Forschung im Ingenieurwesen*, vol. 86, pp. 283–294, 2022.

[3] B. Guilbert, P. Velex, D. Dureisseix, and P. Cutuli, "Modular hybrid models to simulate the static and dynamic behaviour of high-speed thin-rimmed gears," *Journal of Sound and Vibration*, vol. 438, pp. 353-380, 2018.

[4] W. B. Shangguan, X. L. Liu, Y. Yin *and S. Rakheja,* "Modeling of automotive driveline system for reducing gear rattles," *Journal of Sound and Vibration*, vol. 416, pp. 136-153, 2018.

[5] Y. Mao, P. Borghesani, Z.Y. Chin, and RB. Randall, Z. Peng, "Extraction and use of frequency-domain relationships between time-varying gear meshing properties and diagnostic measurements," *Mechanical Systems and Signal Processing*, vol. 190, p. 110129, 2023.

[6] A. Kahraman, and R. Singh, "Nonlinear dynamics of a geared rotor-bearing system with multiple clearances," *Journal of Sound and Vibration*, vol. 144, no. 3, pp. 469-506, 1991.

[7] D. P. Sheng, R. P. Zhu, G. H. Jin, F-X. Lu, and H-Y. Bao, "Bifurcation and chaos study on transverse-torsional coupled 2K-H planetary gear train with multiple clearances," *Journal of Central South University*, vol. 23, pp. 86-101, 2016.

[8] M. Azimi, "Pitchfork and Hopf bifurcations of geared systems with nonlinear suspension in permanent contact regime," *Nonlinear Dynamic*, vol. 107, pp. 3339-3363, 2022.

[9] M. Abruzzo, M. Beghini, C. Santus, and S. Manconi, "Dynamic behavior of a power re-circulating gear test rig including periodic variation of mesh stiffness and static transmission error," *Mechanism and Machine Theory*, vol. 159, 104247, 2021.

[10] N. Ullah, T. Cong, B. Huan, and H. Yucheng, "Influence of optimal tooth modifications on dynamic characteristics of a vehicle gearbox," *International Journal of Automotive and Mechanical Engineering*, vol. 16, no. 1, pp. 6319-6331, 2019.

[11] H. Motahar, F.S. Samani, and M. Molaie, "Nonlinear vibration of the bevel gear with teeth profile modification," *Nonlinear Dynamic*, vol. 83, pp. 1875–1884, 2016.

[12] Y. Xia, Y. Wan, and Z. Liu, "Bifurcation and chaos analysis for a spur gear pair system with friction," *Journal of the Brazilian Society of Mechanical Sciences and Engineering*, vol. 40, p. 529, 2018.

[13] Q. R. Zhao, X. Wang, T. T. Li, and H. Zhang, "Analysis of coupling fault correlation and nonlinear vibration of multi-stage gear transmission system," *Journal of Vibroengineeering*, vol. 23, no. 7, pp. 114-126, 2020.

[14] E. Rigaud, and J. Perret-Liaudet, "Investigation of gear rattle noise including visualization of vibro-impact regimes," *Journal of Sound and Vibration*, vol. 467, 115026, 2020.

[15] G. Martynenko, "Resonance mode detuning in rotor systems employing active and passive magnetic bearings with controlled stiffness," *International Journal of Automotive and Mechanical Engineering*, vol. 13, no. 2, pp. 3293-3308, 2016.

[16] A. Saghafi, and A. Farshidianfar, "An analytical study of controlling chaotic dynamics in a spur gear system," *Mechanism and Machine Theory*, vol. 96, pp. 179-191, 2016.

[17] A. Donmez, and A. Kahraman, "Characterization of nonlinear rattling behavior of a gear pair through a validated torsional model," *Jounal of Computational and Nonlinear Dynamic*, vol. 17, no. 4, p. 041006, 2022.

[18] G. Arian, and S. Taghvaei, "Dynamic analysis and chaos control of spur gear transmission system with idler," *European Journal of Mechanics - A/Solids*, vol. 87, no. 1, p. 104229, 2021.

[19] A. Farshidianfar, and A. Saghafi, "Global bifurcation and chaos analysis in nonlinear vibration of spur gear systems," *Nonlinear Dynamics*, vol. 75, no. 4, pp. 783-806, 2014.

[20] J. F. Mason, P. T. Piiroinen, R. E. Wilson, and M. Homer, "Basins of attraction in non-smooth models of gear rattle," *International Journal of Bifurcation and Chaos*, vol. 19, no. 1, pp. 203-224, 2009.

[21] X. F. Gou, L. Y. Zhu, and D. L. Chen, "Bifurcation and chaos analysis of spur gear pair in two-parameter plane," *Nonlinear Dynamics*, vol. 79, no. 3, pp. 2225-2235, 2015.

[22] C. Padmanabhan, R. C. Barlow, T. E. Rook, and R. Singh, "Computational issues associated with gear rattle analysis," *Journal of Mechanical Design*, vol. 117, no. 1, pp. 185-192, 1995.

[23] Z. H. Hu, J. Y. Tang, Q. S. Wang, S. Chen and L. Qian, "Investigation of nonlinear dynamics and load sharing characteristics of a two-path split torque transmission system," *Mechanism and Machine Theory*, vol. 152, p. 103955, 2020.

[24] S. Qiao, J. Zhou, X. Zhang, and H. Jiang, "Dynamic thermal behavior of two-stage gear transmission system," *Journal of Vibration Engineering and Technologies*, vol. 9, pp. 1809–1831, 2021.